Int J Adv Manuf Technol (2015) 77:1281–1293
DOI 10.1007/s00170-014-6563-3

ORIGINAL ARTICLE

A new process of forming metallic bipolar plates for PEM fuel cell with pin-type pattern

M. Belali-Owsia · M. Bakhshi-Jooybari · S. J. Hosseinipour · A. H. Gorji

Received: 9 March 2014 / Accepted: 28 October 2014 / Published online: 7 November 2014

Abstract Bipolar plates are the most important and expensive components of a fuel cell. These plates can be fabricated by different processes, such as machining graphite plates, producing composite materials, and forming metallic sheets. Due to some benefits of the metallic plates, especially with stainless steel sheets, they have recently been more noticeable. There are various flow field patterns with different applications in these plates, being classified into simple and complex ones in forming process for spiral or parallel and multi-array pin-type examples, respectively. In this study, hydroforming, stamping, and hybrid hydroforming–stamping methods have been used to investigate the forming capability of multi-array pin-type pattern, and, consequently, to compare the results of filling percentage and thickness distribution of these methods. According to the results, samples formed by the hybrid method have shown desirable filling percentage and thickness distribution. The effect of preload pressure of this method on thickness distribution has subsequently been studied and it was observed that the thickness distribution of the formed sample was enhanced by maximizing the pressure of the hydroforming stage.

Keyword Sheet metal forming · Metallic bipolar plates · Hydroforming · Hybrid method · Stamping

M. Belali-Owsia · M. Bakhshi-Jooybari (✉) · S. J. Hosseinipour · A. H. Gorji
Metal Forming Research Group, Babol University of Technology, Babol, P.O. Box 484, Mazandaran, Iran
e-mail: bakhshi@nit.ac.ir

1 Introduction

Bipolar plates are an important component of fuel cells. The selection of plate material, the geometrical design of flow field on the plate, and the manufacturing technique are the main elements in the production of fuel cells. In recent years, there has been a great interest in proton exchange membrane (PEM) fuel cells due to their high efficiency, fast startup, high potential for energy conservation, safety, and environmental protection. PEM fuel cell is the main candidate to replace the internal combustion engine in transportation applications [1, 2]. Different types of material such as: (1) graphite plates [3, 4], (2) composite plates (polymer–graphite composite plates [5–7] and carbon/carbon composite plates) [8], (3) metal foam plates [9], and (4) metallic plates [10–15] have been utilized in order to produce bipolar plates, as shown in Fig. 1.

Metallic bipolar plates, especially stainless steel plates, have recently received considerable attention due to their low cost, excellent mechanical, electrical, and thermal properties, as well as good manufacturability [19–21].

As the primary difficulty in manufacturing the metallic bipolar plate is the formation of the microchannel, in recent years, several techniques for the production of metallic bipolar plates have been developed. Liu et al. [22], for example, studied the feasibility of rubber pad forming in the production of metallic bipolar plates and the effects of forming parameters. The results showed that a convex die is suitable for narrow channels, whereas a concave die is appropriate for wide channels. A group of collaborators consisting of American Trim, the Ohio State University, and General Motors [23] commercially developed a viable prototype production

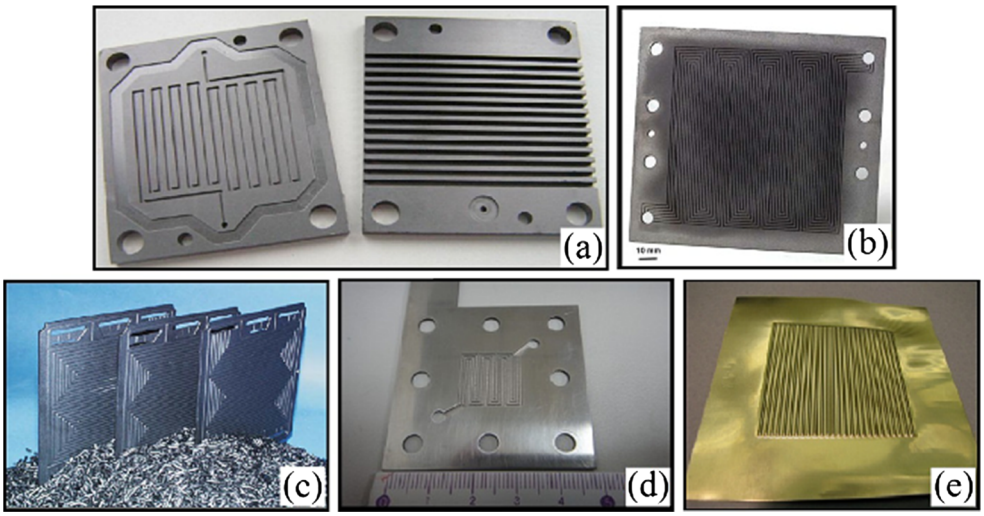

Fig. 1 Different production types of a bipolar plate: **a** machined graphite [16], **b** molded carbon/carbon material [8], **c** molded polymer/carbon composite [17], **d** micro EDM stainless steel [18], and **e** forming stainless steel [10]

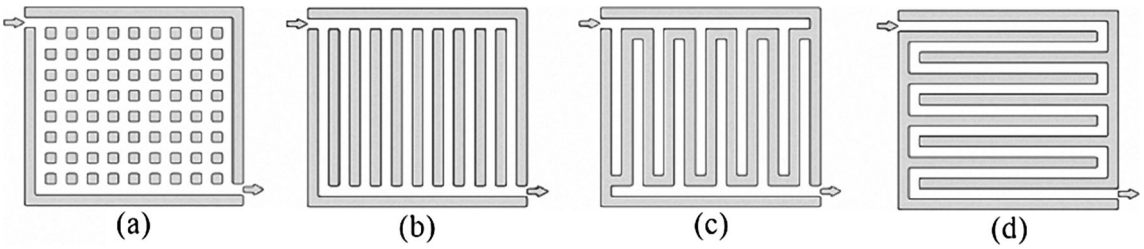

Fig. 2 Schematic illustration of the main flow fields: **a** pin-type, **b** parallel channels, **c** serpentine, and **d** interdigitated [25]

process to manufacture metallic fuel cell bipolar plates in which electromagnetic coils and forming dies were integrated. Koc and Mahabunphachai [19, 20, 24] also investigated the formation of metallic bipolar plates by hydroforming process.

In design and manufacture of bipolar plates, different types of flow fields are used in order to achieve the best efficiency in various usages. Since it is not possible to obtain fully homogeneous conditions over the entire active electrode area with respect to temperature, reactant concentrations, and humidity, a compromise has to be made [25]. Heinzel et al. [25] examined different kinds of flow fields and classified them into four types, as illustrated in Fig. 2. Lobato et al. [26, 27] investigated these flow fields and concluded that the pin-type channel can be used when working at the high temperature without expecting lower performance. Pressure drop caused by pin-type flow channel will also be the lowest of the four geometries tested.

In recent years, a multitude of studies have been carried out on forming different types of flow fields, however, they are mainly limited to the formation of serpentine pattern. So far, no report has been discovered on forming metallic bipolar plates with pin-type flow field.

In this paper, forming stainless steel bipolar plates with pin-type flow field has been simulated with the FEM software, ABAQUS 6.10. After verifying the results, three processes of hydroforming, stamping and hybrid hydroforming–stamping have been studied with the simulation software. The most appropriate process has been selected based on the best filling percentage, thickness distribution, and shape of desired flow field. After selecting the best forming method, the effect of preload pressure has also been studied.

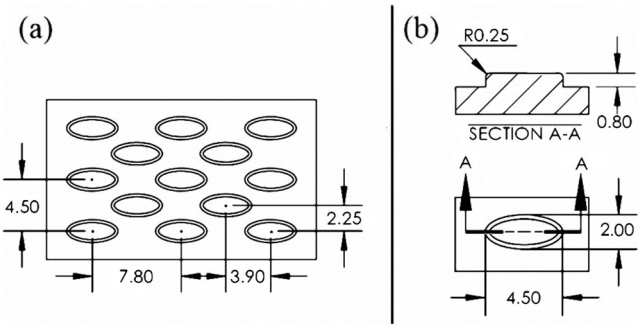

Fig. 3 **a** Pattern of flow field and **b** dimensions of pins

Table 1 Chemical composition of SS304 sheet metal (wt%)

Fe	C	Mn	Cr	Ni	Mo	Co	P	S	Si	Cu	V	Al
Balance	0.064	1.29	18.1	8.85	0.19	0.08	0.03	0.005	0.31	0.27	0.096	0.001

2 Experimental setup and methodology

The multi-array pin-type flow field studied in this research is shown in Fig. 3.

The sheet metal used in this paper was austenitic stainless steel 304 with the thickness of 0.11 mm. The chemical composition of the sheet is shown in Table 1. The mechanical properties of the stainless steel 304 sheet are shown in Table 2 and the true stress–strain curve is presented in Fig. 4, which is estimated by Eq. (1).

$$\sigma = K\left(\varepsilon_0 + \overline{\varepsilon}_{\mathrm{p}}\right)^n \tag{1}$$

Figure 5 illustrates the schematic of the die set used in this research. It consists of upper die, lower die, and die insert. The die insert was made of brass and the upper and lower dies were made of tool steel DIN 2080. The pattern was machined on the die insert with a CNC machine.

The pressure path applied in the experiments is shown in Fig. 6. Fig. 7 shows the equipment for forming metallic bipolar plates with the die set installed. It consists of a 40-ton hydraulic press and a pressure unit with 140-MPa pressure capacity.

3 Numerical simulation

For the simulation of the process, ABAQUS 6.10 software was used. The mechanical properties of the stainless steel 304 sheet shown in Table 2 were introduced to the software. In the simulation, the behavior of sheet metal was assumed to be isotropic and modeled as a 3D deformable shell element. The die set was also modeled as 3D discrete rigid element. As shown in Fig. 8, due to geometrical symmetry in both longitudinal and transverse directions, the geometry of the modeled die consists of one ellipse with four quarters of adjacent ellipses.

Table 2 Mechanical properties of SS304 sheet

Young's modulus, E (GPa)	196
Poisson's ratio, ν	0.3
Yield stress, σ_y (MPa)	255
K (MPa)	1505
n	0.65
ε_0	0.06

The friction coefficients between the sheet and die for hydroforming process and for stamping process were selected as 0.1 [21] and 0.15 [28], respectively. The boundary condition of the sheet was symmetric at edges along the longitudinal and transverse directions, and free along the altitude. To mesh the elements, quad-dominated mesh with the size of 0.03 mm was used. After the parameters were introduced, the three selected processes of (i) hydroforming, (ii) stamping, and (iii) hybrid hydroforming–stamping were modeled in the simulation software as shown in Fig. 9.

4 Results and discussion

In order to implement the study, the results of filling percentage and thickness distribution in longitudinal, transverse, and diagonal directions were compared. These directions are shown in Fig. 10.

4.1 Validation of FEM model

Figure 11 illustrates both top and bottom view of experimental and simulation results of the hydroformed samples with 13 pins at 80 MPa pressure.

The criterion presented by Liu et al. [22] was used to investigate the filling percentage (% filling). To measure the filling percentage for both narrow and wide channels, the

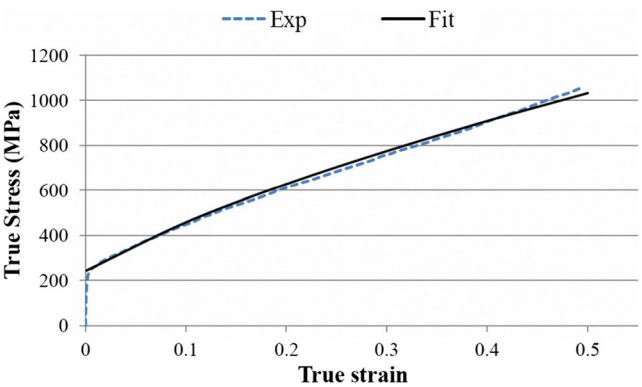

Fig. 4 True stress–true strain curve of SS304

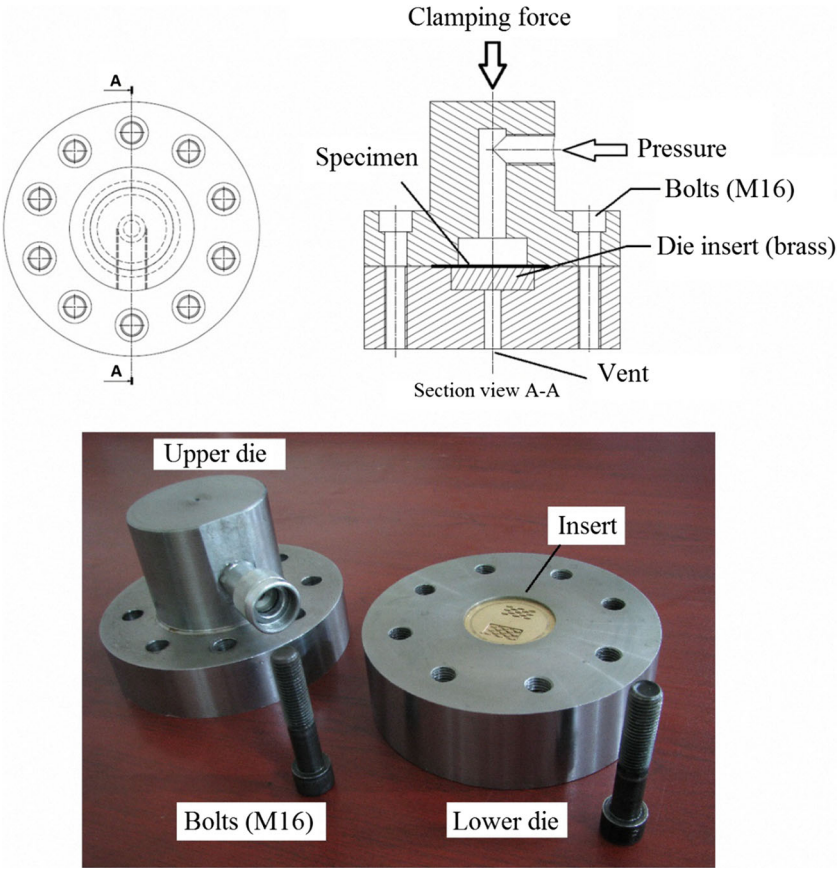

Fig. 5 Main components of the die set

ratios of d/D or l/L were used, respectively, as shown in Fig. 12. This criterion is defined as follows:

$$\%\text{filling} = (d/D) \times 100 = (l/L) \times 100 \quad (2)$$

Where d and D are the depth of the formed sample and that of the die channel, respectively, and l and L are the instantaneous contact length and maximum contact length of the formed sample with the die, respectively.

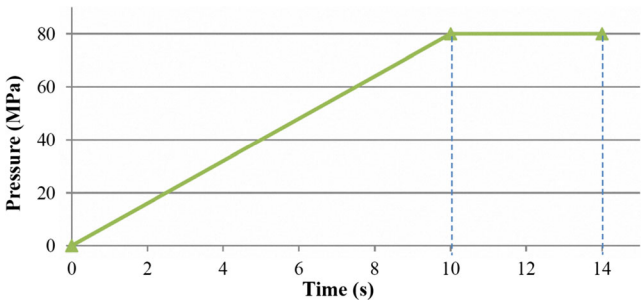

Fig. 6 Pressure path utilized to form the samples

Fig. 7 Photograph of the experimental forming setup

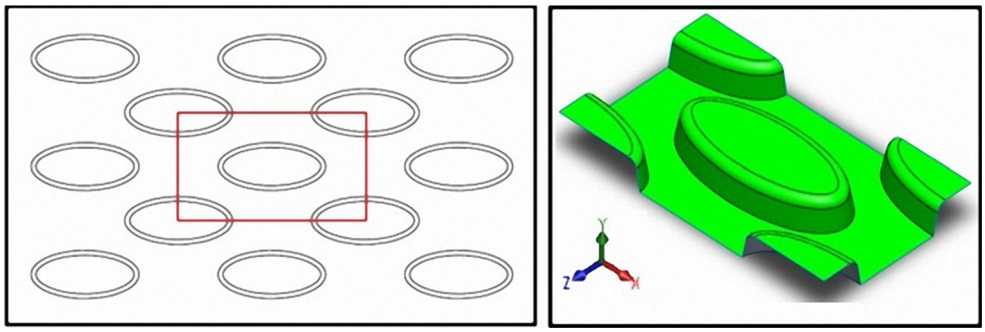

Fig. 8 Schematic diagram of the die model for simulation in ABAQUS software

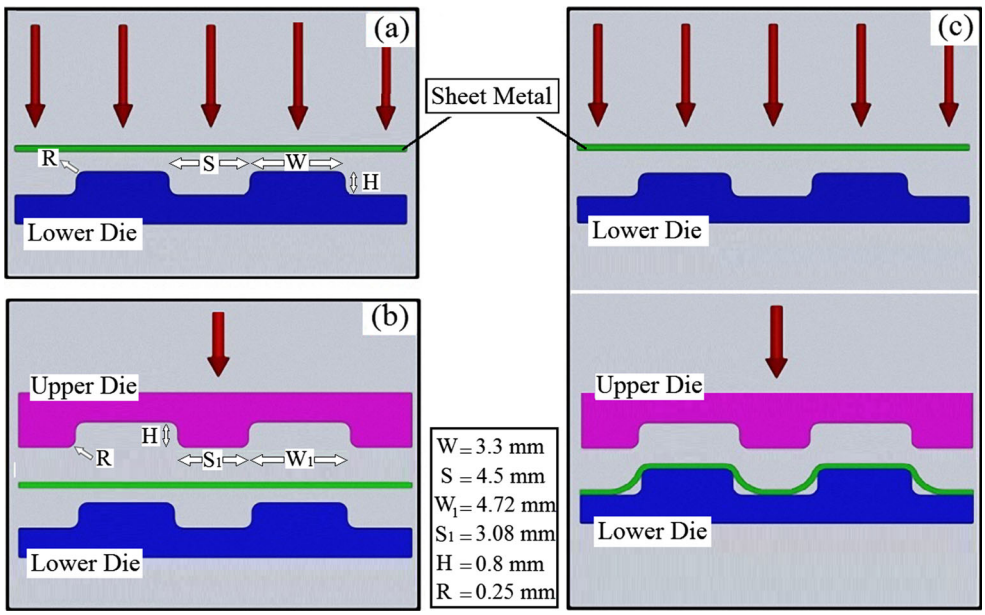

Fig. 9 **a** Hydroforming, **b** stamping, **c** hybrid hydroforming-stamping (modeled in the software)

Figure 13 shows the sections of the hydroformed samples in transverse, longitudinal, and diagonal directions. The simulation results obtained for filling percentage in different directions were close to those of the experimental ones, as shown in Fig. 14.

Figure 15 illustrates the thickness distribution of the hydroformed part in different directions, obtained from experiments and simulations. As can be seen, the results are generally in agreement.

Based on refs. [29, 30], the maximum thinning was considered as a fracture criterion in the simulations. According to the process stated in the above references, the maximum thinning was obtained at 0.062 mm which is in close agreement with the exper-

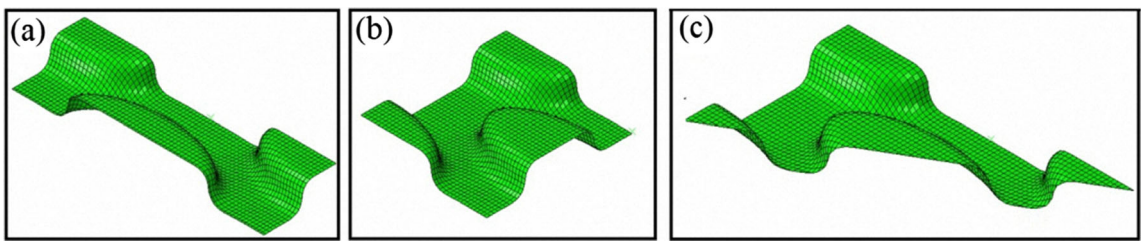

Fig. 10 Three investigated sections: **a** longitudinal, **b** transverse, and **c** diagonal

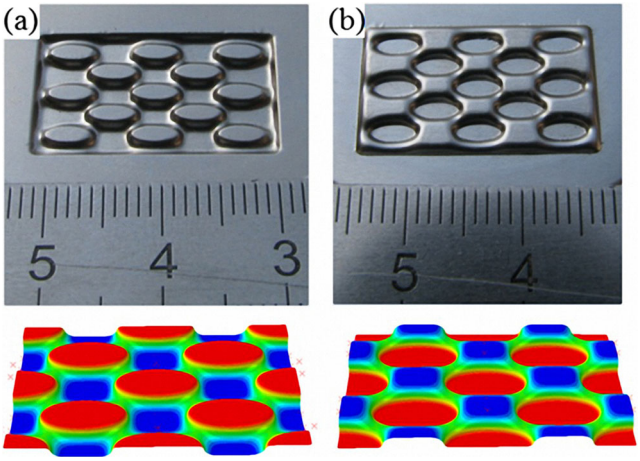

Fig. 11 The **a** top and **b** bottom views of hydroformed parts resulting from experiments and simulations

imental finding that was 0.06 mm. Therefore, the value of 0.062 mm was selected as the fracture criterion in the simulations.

4.2 Filling percentage

Due to the nature of the stamping and hydroforming–stamping processes in which rigid tools are used, at the final stage of forming, the dies will be filled (or nearly filled) if the formed part are able to be safely produced. In contrast, in the hydroforming process under investigation, the die was not able to be filled completely by the available maximum forming pressure. Figure 16 shows the variation of filling percentage in the hydroforming process with respect to the forming pressure. As it is seen, by increasing the filling percentage, the required pressure is increased exponentially. Thus, to obtain the fully filled profile, very high pressure is required. This point has been reported in the research works performed by Mahabanphachai et al. [24] and Hung et al. [31]. As a result, the die cannot be fully filled in the hydroforming method.

Figure 17 shows the cross-sections of the hydroformed and stamped samples in the longitudinal, transverse, and diagonal directions. The filling percentage of the two samples correspond to the different

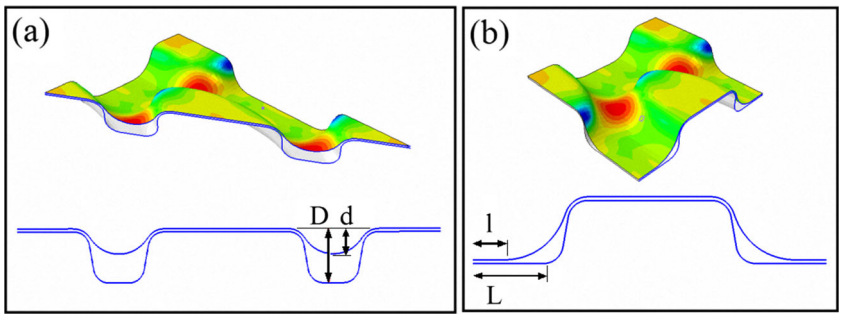

Fig. 12 Definition of the filling percentage: **a** *d*/*D*, and **b** *l*/*L*

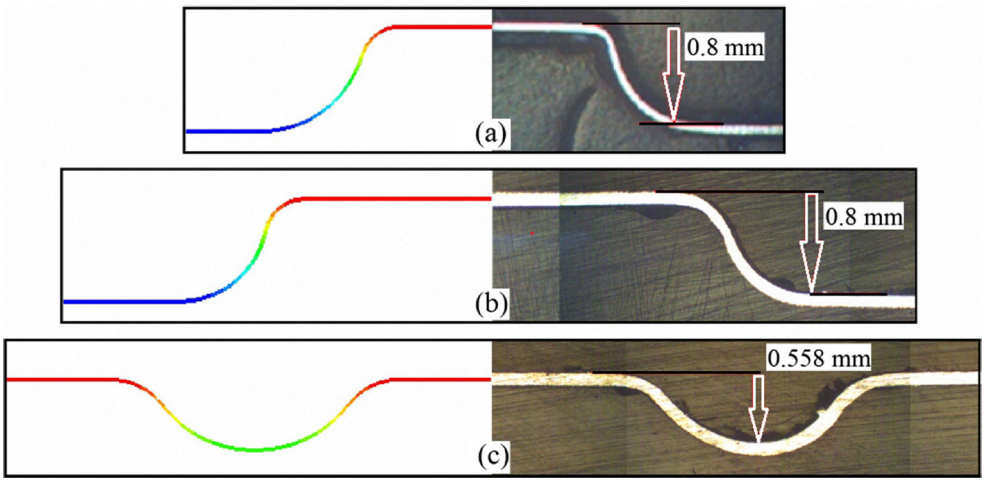

Fig. 13 **a** Transverse, **b** longitudinal, and **c** diagonal comparisons of the depth of the hydroformed pattern, resulting from experiments and simulations

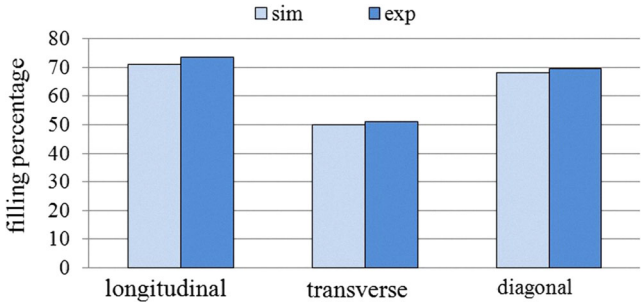

Fig. 14 A comparison of the filling percentage of the hydroformed part at pressure of 80 MPa

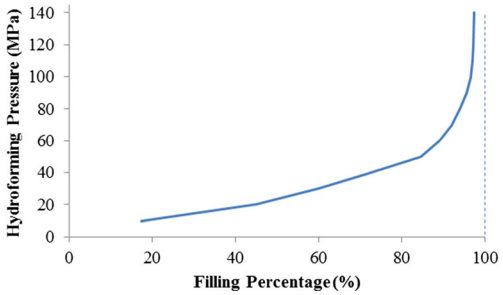

Fig. 16 Variation of the filling percentage in hydroforming process with respect to the forming pressure

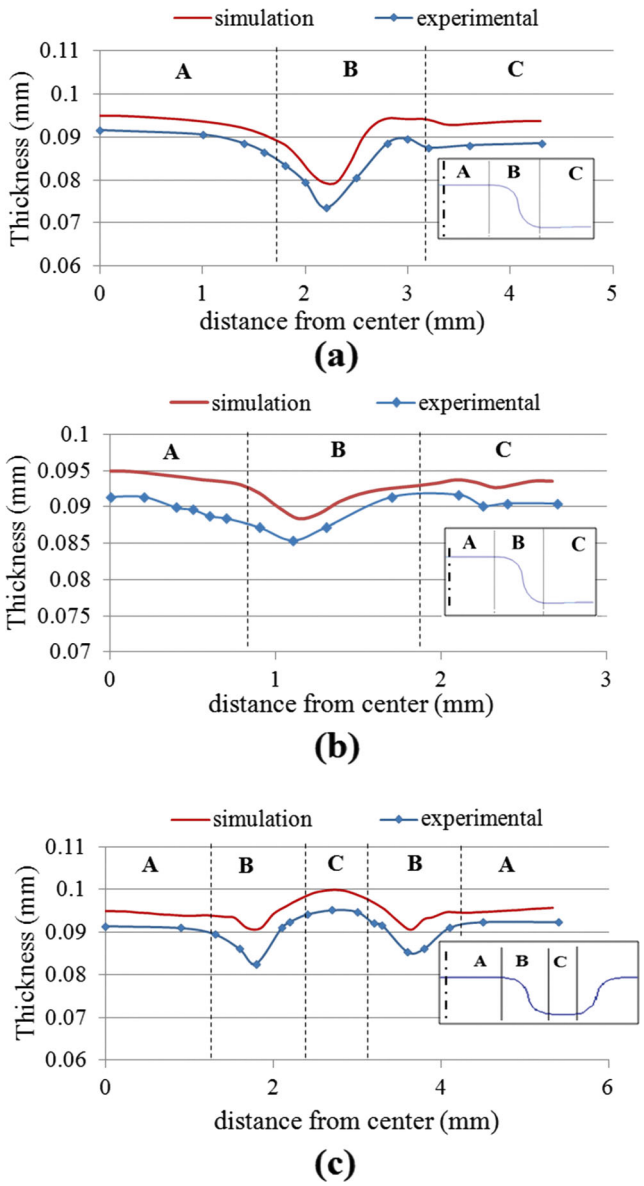

Fig. 15 Thickness distribution of the hydroformed part: **a** longitudinal, **b** transverse, **c** diagonal directions

directions are illustrated in Fig. 18. As it can be seen, in the stamped sample, the die is fully filled in the three directions. In the hydroformed sample, the maximum filling percentage belongs to the longitudinal direction which is 94.3 %. Moreover, in the diagonal and transverse directions, the hydroformed sample has the filling percentage of 63.2 and 75.3 %, respectively. As a result, a stamping stage is required to achieve a fully filled sample.

Based on the simulations performed in this research, it was concluded that due to the sharp corners of the die (pin-type pattern), by increasing the maximum pressure to 140 MPa, the minimum thickness of the sample was reached to the critical thickness. Thus, the 140 MPa pressure was considered as the critical pressure. Therefore, in performing the experiments, the maximum pressure was limited to 120 MPa.

Figure 19 shows the hydroformed and stamped parts together with the corresponding cross-sections in the longitudinal direction with respect to the filling depth. As it is shown, in the stamped sample, the die is nearly filled, whereas in the hydroformed sample, the corners of the die are not suitably filled. Since the pin-type bipolar plate cannot be appropriately formed in the hydroforming process, only stamping and hybrid hydroforming–stamping processes were examined in this paper.

4.3 Thickness distribution

Figure 20 shows the position of bipolar plates in a fuel cell stack. The surface of the bipolar plate is classified into anodic–cathodic surface (zone A), channel wall (zone B), and flow channel floor (zone C). According to Dundar, the plate should have suitable thickness in zone A due to many chemical reactions with MEA[1] and

[1] Membrane electrode assembly.

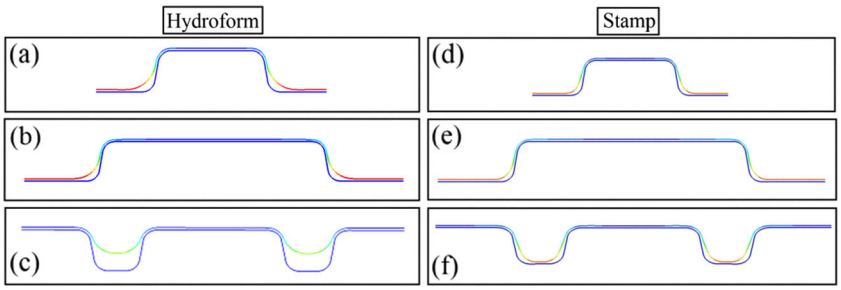

Fig. 17 Cross-sections of the hydroformed and stamped parts corresponding to: **a** and **d** transverse directions, **b** and **e** longitudinal directions, and **c** and **f** diagonal directions

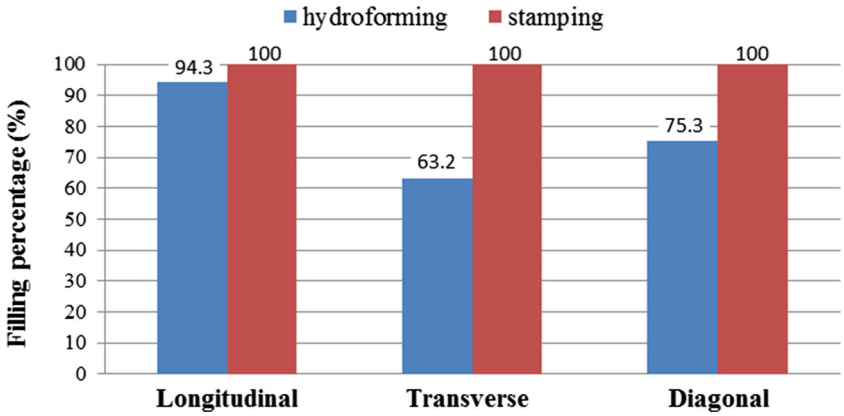

Fig. 18 Filling percentage of the hydroformed part at maximum pressure of 120 MPa and stamped part

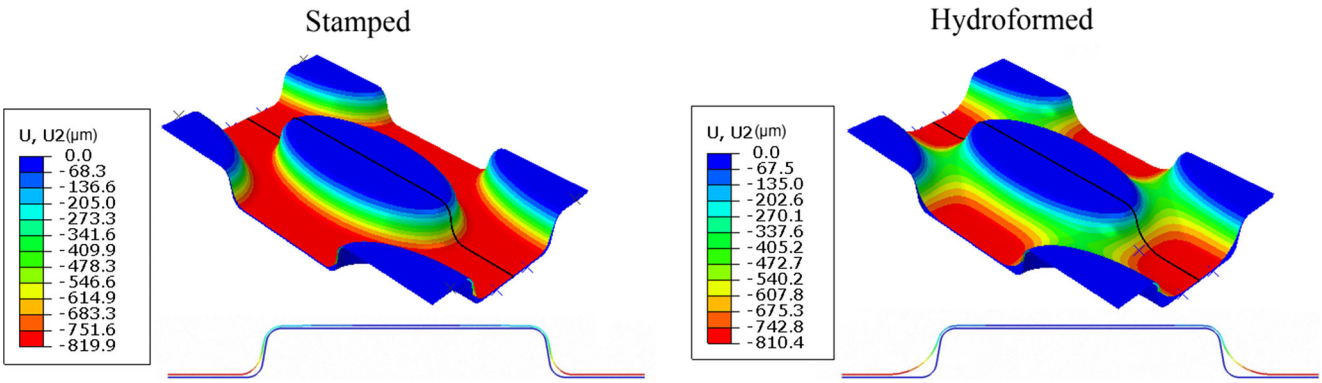

Fig. 19 The hydroformed and stamped parts and the corresponding cross-sections in longitudinal direction, with respect to the filling depth

high corrosion in this zone [32]. Moreover, samples with more uniform thickness in zones A, B, and C will be more desirable.

Figure 21 shows the thickness distribution of the simulated samples in the longitudinal, transverse, and diagonal directions by the hybrid method and stamping. As it is seen, the thickness distribution in the hybrid method is more uniform than in the stamping. In addition, in the hybrid method, the maximum thickness reduction in the critical zone B is much less than that of the stamping process. In Fig. 21, the fracture criterion (0.062 mm) is shown by a dashed line. As can be seen, in the critical zone B, the thickness of the stamped sample in the longitudinal and transverse

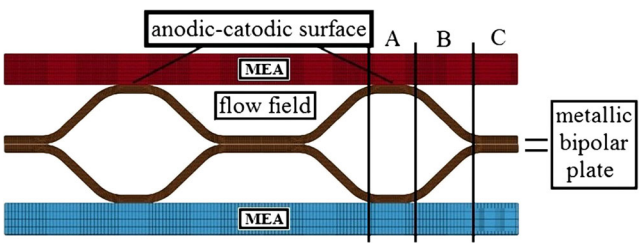

Fig. 20 Schematic arrangement of the bipolar plate in the PEM fuel cell stack

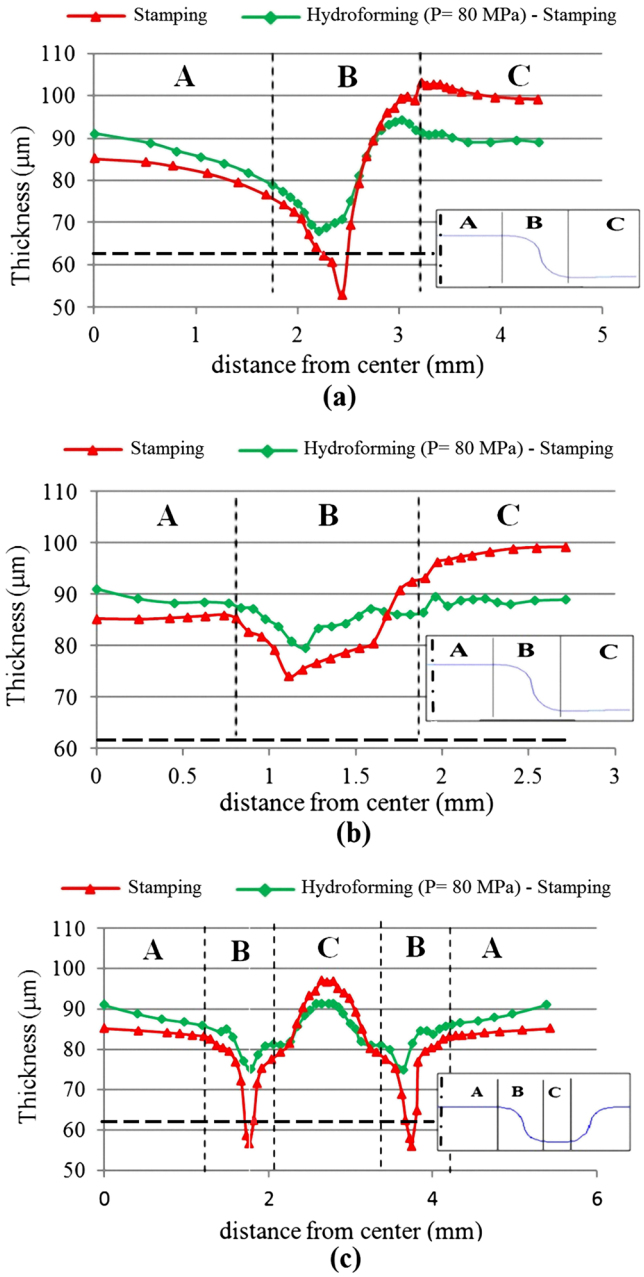

Fig. 21 Thickness variation of the formed part in: **a** longitudinal, **b** transverse, **c** diagonal sections obtained from the simulation

directions are lower than the fracture line. Thus, it can be concluded that the stamped sample is ruptured in the critical zone, whereas the thickness in the hybrid method in all directions is above the fracture line. These results can be achieved from Fig. 22 that show the thickness distribution of the deformed parts obtained by the simulation for the hybrid method and stamping. The main reason worth notifying is that in the stamping process, the rigid die contacts the sheet from the start of the process. This causes local thinning at the sharp corners (zone B) of the deformed sample. The local thinning prevents proper stretching of the sheet in the other zones.

Since the sample formed by the hybrid method have more filling percentage and lower maximum pressure rather than the hydroformed sample (Figs. 16, 17, and 18) and have more desirable thickness distribution rather than the stamped sample (Figs. 21 and 22), it can be concluded that the hybrid method is more suitable for forming the bipolar plates. Although the disadvantage of the hybrid method is increasing the process working time, but by using this method, the maximum pressure is highly decreased compared to the hydroforming method. This reduces the cost of the equipment and increases the safety of the process.

4.4 Effects of fluid maximum pressure in the hydroforming stage on the thickness distribution in the hybrid method

As stated above, the best process for forming the pin-type bipolar plate is the hybrid hydroforming–stamping method. In this section, the effect of fluid maximum pressure on the thickness distribution of the final part was examined. In this respect, the samples were hydroformed at 40, 80, and 120 MPa maximum pressures and then stamped. In Fig. 23, the thickness distribution curves obtained by simulating the hybrid method in the longitudinal, transverse, and diagonal directions are shown. Generally, the thickness of the most critical

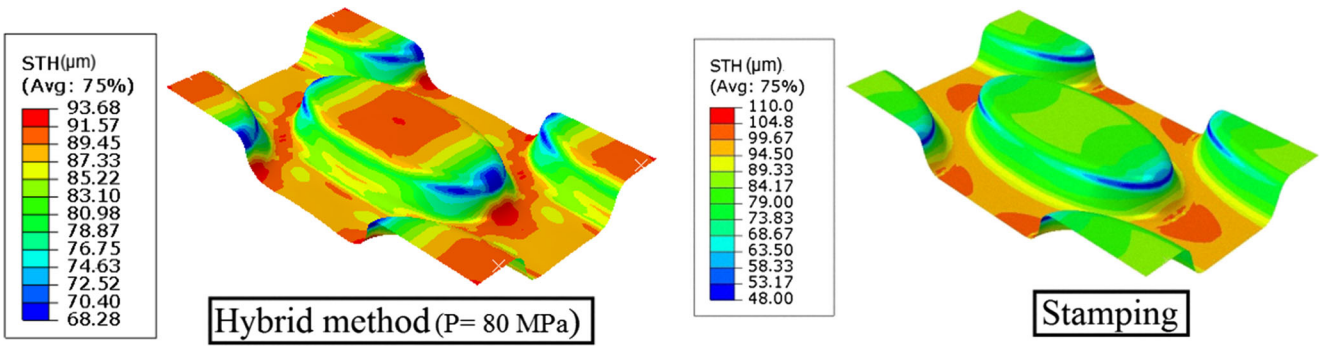

Fig. 22 Thickness variations of the simulated samples formed by the hybrid method (80 MPa pressure and stamping

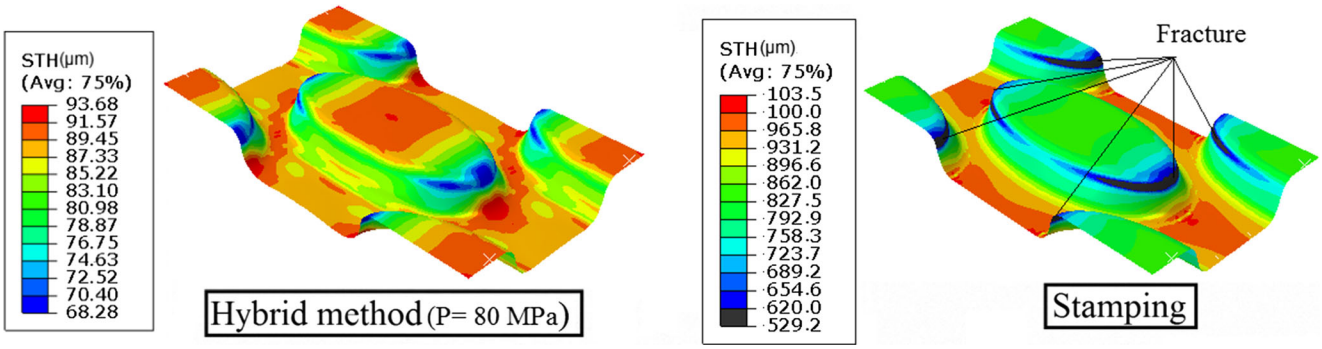

Fig. 23 Thickness variations of the formed part in: **a** longitudinal, **b** transverse, and **c** diagonal sections, obtained from the simulation

region (i.e., the thinnest section at zone B) increases as the pressure rises. Moreover, by increasing the pressure, the thickness in the zone A (anodic–cathodic surface) enhances, which is desirable.

Figure 24 shows the plastic strain distribution of the formed sample with 40 MPa maximum pressure in the longitudinal direction. As it is observed, after the hydroforming stage, the die is not filled (Fig. 24a).

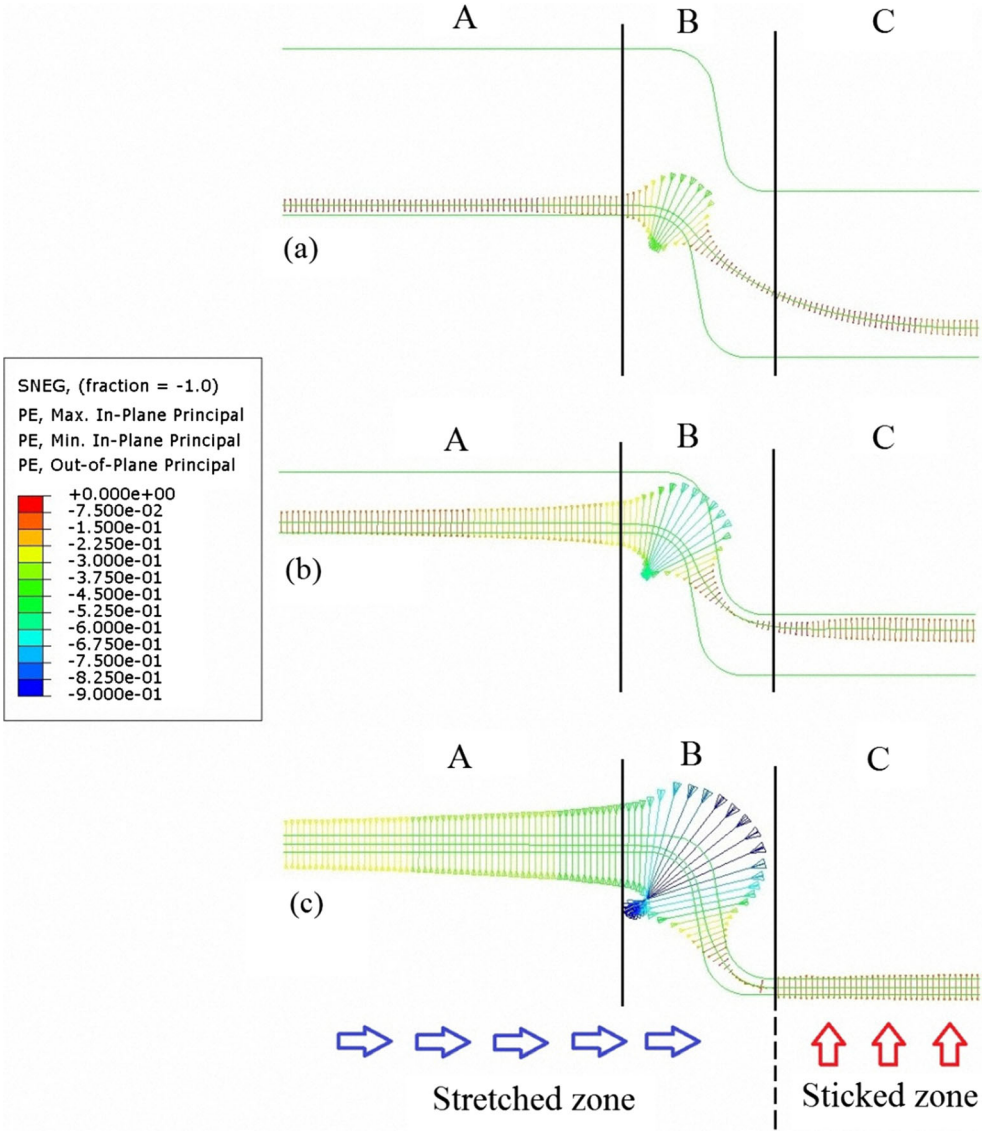

Fig. 24 Plastic strain of the formed sample with 40 MPa maximum pressure in the longitudinal direction: **a** hydroformed, **b** contact between die and sample during stamping stage, and **c** stamped

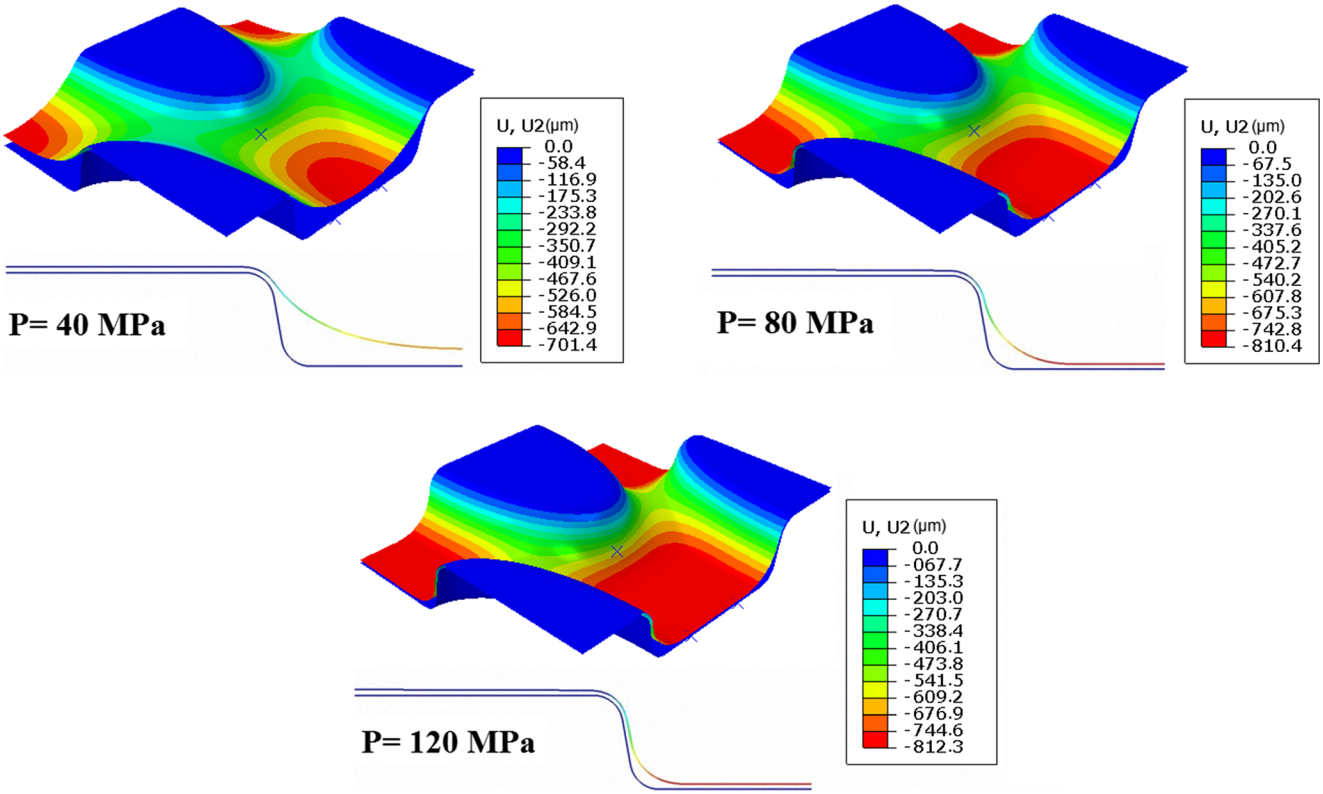

Fig. 25 Depths of filling contour of the samples in the hydroforming stage for different maximum fluid pressures

Therefore, a sizing operation (stamping) is required. In the stamping process, the upper die moves downward and its surface (in zone C) contacts the sample (Fig. 24b). It should be mentioned that the sample stretches due to the lack of radial feeding. In addition, as shown in Fig. 24b, c, the movement of the die does not affect the variation of strain because of the friction between the upper die surface and the sample in the

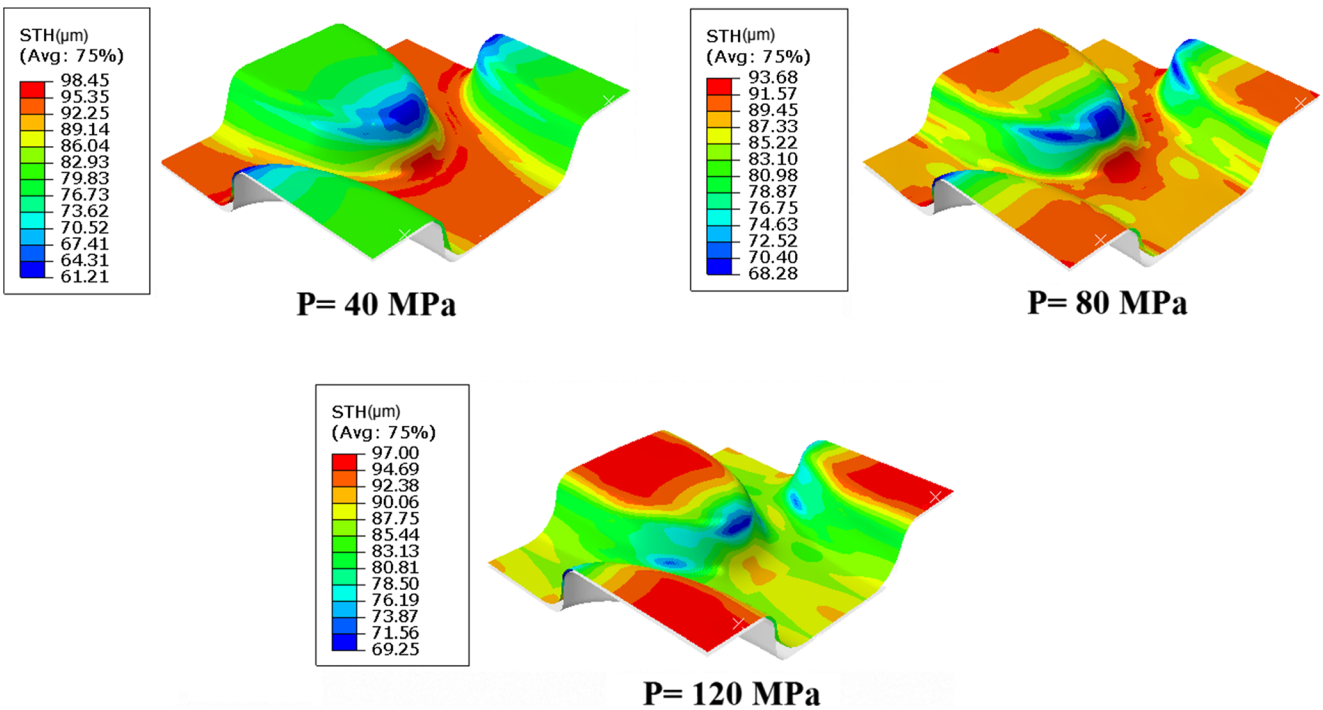

Fig. 26 Thickness distribution contour in the hybrid method for different maximum pressures

zone C. As a result, stretching occurs in the zones A and B and the plastic strain increases, especially in the zone B. Based on the aforementioned reasons, the zones A and B are stretched zones, while the zone C is a zone where the sheet material sticks on Fig. 24c. This behavior occurs in the transverse and diagonal directions as well.

In order to prevent thinning and stretching of the formed samples in the stamping stage, most of the required forming operation on the workpiece should be performed in the hydroforming stage. Figure 25 shows the depth of filling contour of the hydroformed samples at 40, 80, and 120 MPa maximum pressures in the longitudinal direction. As it is seen, the formed samples are gradually fitted to the die by increasing the fluid pressure in the hydroforming stage.

Figure 26 shows the thickness distribution contour of the deformed part obtained by simulation. As it is seen, by increasing the fluid pressure, the thicknesses of the anodic–cathodic surface (upper surface of the pin) and the critical zone (corner of the pin) increases, and, generally, the thickness becomes more uniform. For example, the formed sample with 120 MPa maximum pressure contains more uniform thickness compared to the other two.

5 Conclusion

In this paper, three processes of metal forming were investigated in order to form the metallic bipolar plates with pin-type pattern (complex pattern). At first, the hydroforming method was simulated by the FE model. Then, the experiments were performed for the verification of FE model. After the verification, these three processes were investigated in order to select the best forming processes of metallic bipolar plates. In this investigation, the filling percentage and thickness distribution of the metallic bipolar plate were studied after forming. Among these three processes (hydroforming, stamping, and hybrid method), the metallic bipolar plate formed by the hybrid hydroforming–stamping process has shown desirable filling percentage and thickness distribution. Afterward, the effect of maximum pressure in the hydroforming stage was studied and observed that when the maximum pressure of the hydroforming stage rises, the critical zone becomes less thinner and the formed sample reaches more uniform thickness distribution. Using the hybrid method, the metallic bipolar plate with pin-type pattern could be completely formed without rupture, with uniform thickness and a thicker area in the anodic–cathodic surface of the bipolar plate.

References

1. Tawfik H, Hung Y, Mahajan D (2007) Metal bipolar plates for PEM fuel cell—a review. J Power Sources 163:755–767
2. Liu Y, Hua L (2010) Fabrication of metallic bipolar plate for proton exchange membrane fuel cells by rubber pad forming. J Power Sources 195:3529–3535
3. Cunningham B, Baird D-G, Mater J (2006) The development of economical bipolar plates for fuel cells. Chem 16:4385–4388
4. Middelman E, Kout W, Vogelaar B, Lenssen J, De Waal E (2003) Bipolar plates for PEM fuel cells. J Power Sources 118(1–2):44–46
5. Oh M-H, Yoona Y-S, Park S-G (2004) The electrical and physical properties of alternative material bipolar plate for PEM fuel cell system, J. Electrochim Acta 50:777–780
6. Cho E-A, Jeon U-S, Ha H-Y, Hong S-A, Oh I-H (2004) Characteristics of composite bipolar plates for polymer electrolyte membrane fuel cells. J Power Sources 125:178–182
7. Kuan H-C, Ma C-C-M, Chen K-H, Chen S-M (2004) Preparation, electrical, mechanical and thermal properties of composite bipolar plate for a fuel cell. J Power Sources 134:7–17
8. Besmann T, Henry J, Lara-Curzio E, Klett J-W, Haack D, Butcher K (2003) Pro Mater Res Soc Symp 756:415–422
9. Arisetty S, Prasad A-K, Advani S-G (2007) Metal foams as flow field and gas diffusion layer in direct methanol fuel cells. J Power Sources 165:49–57
10. Peker M-F (2012) Investigations on the micro-scale surface interactions at the tool and workpiece interface in micro-manufacturing of bipolar plates for proton exchange membrane fuel cells, Doctor of Philosophy at Virginia Commonwealth University
11. Wang S-H, Peng J, Lui W-B, Zhang J-S (2006) Performance of the gold-plated titanium bipolar plates for the light weight PEM fuel cells. J Power Sources 162:486–491
12. Wang H, Sweikart M-A, Turner J-A (2003) Stainless steel as bipolar plate material for polymer electrolyte membrane fuel cells. J Power Sources 115:243–251
13. Lim S-S, Kim Y-T, Kang C-G (2011) Fabrication of aluminum 1050 micro-channel proton exchange membrane fuel cell bipolar plate using rubber-pad-forming process. Int J Adv Manuf Technol. doi:10.1007/s00170-012-4162-8
14. Kwon H-J, Jeon Y-P, Kang C-G (2011) Effect of progressive forming process and processing variables on the formability of aluminium bipolar plate with microchannel. Int J Adv Manuf Technol. doi:10.1007/s00170-012-4033-3
15. Palumbo G, Piccininni A (2013) Numerical–experimental investigations on the manufacturing of an aluminium bipolar plate for proton exchange membrane fuel cells by warm hydroforming. Int J Adv Manuf Technol. doi:10.1007/s00170-013-5047-1
16. http://mgmcarbon.en.ec21.com/Products–3059727.html
17. Muller A, Kauranen P, von Ganski A, Hell B (2006) Injection moulding of graphite composite bipolar plates. J Power Sources 154:467–471
18. Hung J-C, Yang T-C, Li K-C (2011) Studies on the fabrication of metallic bipolar plates—using micro electrical discharge machining milling. J Power Sources 196:2070–2074
19. Mahabunphachai S (2008) A hybrid hydroforming and mechanical bonding process for fuel cell bipolar plates, Doctor of Philosophy (Mechanical Engineering) in The University of Michigan
20. Koc M, Mahabunphachai S (2007) Feasibility investigations on a novel micro-manufacturing process for fabrication of fuel cell bipolar plates: Internal pressure-assisted. J Power Sources 172:725–733
21. Peng L, Liu D, Hu P, Lai X, Ni J (2010) Fabrication of metallic bipolar plates for proton exchange membrane fuel cell by flexible forming process-numerical simulations and experiments. J Fuel Cell Sci Technol 7:031009–1

22. Liu Y, Hua L, Lan J, Wei X (2010) Studies of the deformation styles of the rubber-pad forming process used for manufacturing metallic bipolar plates. J Power Sources 195:8177–8184
23. Shang J, Wilkerson L, Hatkevich S, Daehn G-S (2010) Commercialization of fuel cell bipolar plate manufacturing by electromagnetic forming, The Ohio State University, USA; 4th International Conference on High Speed Forming −2010
24. Mahabunphachai S, Koc M (2008) Fabrication of micro-channel arrays on thin metallic sheet using internal fluid pressure: Investigations on size effects and development of design guidelines. J Power Sources 175:363–371
25. Heinzel A, Mahlendorf F, Jansen C (2009) Bipolar plates. Elsevier, Duisburg
26. Lobato J, Canizares P, Rodrigo M-A, Pinar F-J, Ubeda D (2011) Study of flow channel geometry using current distribution measurement in a high temperature polymer electrolyte membrane fuel cell. J Power Sources 196:4209–4217
27. Lobato J, Canizares P, Rodrigo M-A, Pinar F-J, Mena E, Ubeda D (2010) Three-dimensional model of a 50 cm^2 high temperature PEM fuel cell. Study of the flow channel geometry influence. Int J Hydrog Energy 35:5510–5520
28. Silva H-C, Lajarin S-F, Marcondes P-V-P (2010) Analysis of numerically simulated true strain on high stampability sheets. J Braz Soc Mech Sci Eng XXXII:1–21
29. Yingyot AUL, Ngaile G, Altan T (2004) Optimizing tube hydroforming using process simulation and experimental verification. J Mater Process Technol 146:137–143
30. Gorji A, Alavi-Hashemi H, Bakhshi-jooybari M, Nourouzi S, Hosseinipour SJ (2011) Investigation of hydrodynamic deep drawing for conical–cylindrical cups. Int J Adv Manuf Technol. doi:10.1007/s00170-011-3263-0
31. Hung J-C, Lin C-C (2012) Fabrication of micro-flow channels for metallic bipolar plates by a high-pressure hydroforming apparatus. J Power Sources 206:179–184
32. Dundar F, Dur E, Mahabunphachai S, Koc M (2010) Corrosion resistance characteristics of stamped and hydroformed proton exchange membrane fuel cell metallic bipolar plates. J Power Sources 195:3546–3552